

Nebular dominated galaxies in the early Universe with top-heavy stellar initial mass functions

Alex J. Cameron^{1*}, Harley Katz^{1†}, Callum Witten^{2,3},
Aayush Saxena¹, Nicolas Laporte^{3,4}, Andrew J. Bunker¹

¹Department of Physics, University of Oxford, Denys Wilkinson
Building, Keble Road, Oxford, OX1 3RH, UK.

²Institute of Astronomy, University of Cambridge, Madingley Road,
Cambridge, CB3 0HA, UK.

³Kavli Institute for Cosmology, University of Cambridge, Madingley
Road, Cambridge, CB3 0HA, UK.

⁴Cavendish Laboratory, University of Cambridge, Madingley Road,
Cambridge, CB3 9BB, UK.

*Corresponding author(s). E-mail(s): alex.cameron@physics.ox.ac.uk;

†These authors contributed equally to this work.

Abstract

The stellar initial mass function (IMF) impacts nearly all observable properties of galaxies [1], controls the production rate of heavy elements, and governs how much energy is available to regulate galaxy growth. Theoretical work predicts that the high-redshift IMF may be more top-heavy compared to the local Universe, due to higher gas pressures, a higher Cosmic Microwave Background temperature, and lower metallicities [2, 3]. However, direct observational evidence for a top-heavy IMF at high-redshift remains elusive. Here we report the detection of two Lyman- α -emitting galaxies at redshift 5.9 and 7.9 that show evidence for exceptionally top-heavy IMFs. Our analysis of JWST/NIRSpec data demonstrates that these galaxies exhibit spectra which are completely dominated by the nebular continuum. Alongside a clear Balmer jump, we observe a steep turnover in the ultraviolet continuum. Although this feature can be produced by an extremely thick damped Lyman- α system with holes, we show instead that this turnover is two-photon emission from neutral hydrogen. Two-photon emission can only dominate if the ionizing emissivity is $\gtrsim 10\times$ that of a

typical star-forming galaxy. While weak He II emission disfavours ionizing contributions from AGN or X-ray binaries, such radiation fields can be produced in star clusters dominated by low-metallicity stars of $\gtrsim 50 M_{\odot}$, where the IMF is $10 - 30\times$ more top-heavy than typically assumed. Such a top-heavy IMF implies our understanding of star formation in the early Universe and the sources of reionization may need revision.

The detection of numerous Ly α -emitting galaxies at $z > 5.5$ from the JWST Advanced Deep Extragalactic Survey (JADES) was recently reported in [4]. Among this sample we identify one object, JADES-GS+53.12175-27.79763 (GS-NDG-9422 hereafter), at $z = 5.943$, that exhibits a clear spectral discontinuity (Figure 1) of 15.0 ± 0.9 nJy (observed frame) at the location of the Balmer jump ($\lambda_{\text{rest}} = 3645 \text{ \AA}$). This feature arises due to electron recombinations with ionized hydrogen to the first excited state and only appears in spectra of galaxies that contain young stellar populations with high ionizing photon production efficiencies (ξ_{ion}). Balmer jumps have been detected in galaxies at low-redshift [5, 6] and are predicted by numerical simulations [7] and spectral energy distribution (SED) fitting of JWST photometry [8] to be common at high-redshift. In contrast, the other nebular continuum components, free-free and two-photon emission, are predicted to be subdominant compared to the stellar and free-bound contributions in high-redshift spectra.

The subdominance of two-photon emission arises because the ξ_{ion} values of typical low-metallicity stellar populations are not high enough to overcome the steep UV stellar continuum slopes [9]. In contrast, very hot stars, with blackbody temperatures of $\sim 100,000$ K, produce enough ionizing photons to power nebular continuum emission that outshines the stellar UV emission, and are predicted to exhibit a strong two-photon continuum bump, peaking at $\lambda_{\text{rest}} \approx 1430 \text{ \AA}$ [10–12].

In addition to the strong Balmer jump, GS-NDG-9422 exhibits a steep turnover in the continuum at $\lambda_{\text{rest}} \approx 1430 \text{ \AA}$ (Figure 2). Similar UV turnovers are often observed as a result of absorption from foreground neutral hydrogen – either the neutral intergalactic medium (IGM) [13] or a Damped Lyman- α (DLA) system [14]. Fitting GS-NDG-9422 with a typical stellar population requires excess attenuation beyond IGM damping (Figure 2) and necessitates DLA column densities $> 10^{23} \text{ cm}^{-2}$, higher than any known DLA. Furthermore, such high column densities imply zero transmission at 1216 \AA , conflicting with the strong observed Ly α emission. This could be reconciled by invoking a DLA with 30 % leakage (Methods), however the plausibility of such an extreme column density with a low covering fraction is unclear. Furthermore, explaining this with a fine-tuned geometry would seemingly be in tension with the identification of two other objects, the Lynx arc at $z = 3.36$ [15] and a recently-observed galaxy (A2744-NDG-ZD4) from the UNCOVER program [16] at $z = 7.88$, that exhibit a similar turnover in the UV continuum and strong Ly α (Figure 2).

Rather, we argue that, like the Balmer Jump, the observed UV turnover is of nebular origin and a signature of the two-photon continuum arising from $2s \rightarrow 1s$ transitions in neutral hydrogen. To demonstrate this, the top panel of Figure 3 shows

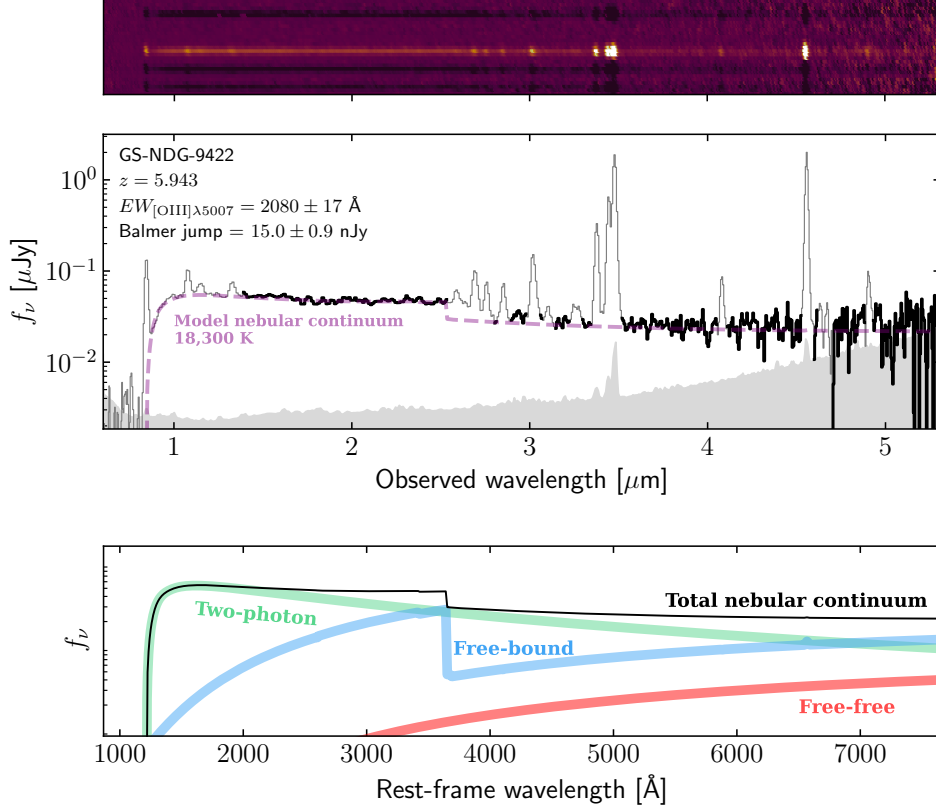


Fig. 1 2D (*top*) and 1D (*middle*) spectra of GS-NDG-9422 showing clear evidence of a spectral break at $2.53 \mu\text{m}$. The grey shaded region shows noise in the observed spectrum, which is well below the signal at the location of the break. *Bottom*: model nebular continuum at 18,300 K showing the relative contribution of the two-photon, free-bound, and free-free components. This model continuum is also shown as the purple dashed line in the middle panel, renormalized to the observed spectrum.

the predicted nebular continuum for gas at a density of 100 cm^{-3} at a range of temperatures. We highlight in magenta the prediction for gas at a temperature of 18,300 K, equal to that measured from $[\text{O III}] \lambda 4363/\lambda 5007$. The fact that the predicted continuum from an independent temperature measurement nearly perfectly matches the observed continuum indicates that the UV turnover is undoubtedly a detection of the two-photon nebular continuum: the spectrum of GS-NDG-9422 is entirely dominated by nebular emission.

In order for both the two-photon and free-bound continua to dominate over the stellar spectrum in the rest-frame UV and optical, the source population must be emitting significantly more ionizing photons than standard SSP models, necessitating blackbody temperatures of $T \gtrsim 90,000 \text{ K}$ (see Methods), much hotter than massive O stars (up to $\sim 50,000 \text{ K}$; [17]). Hence, if the ionizing sources illuminating these three high-redshift galaxies are of stellar origin, they must be exotic in nature.

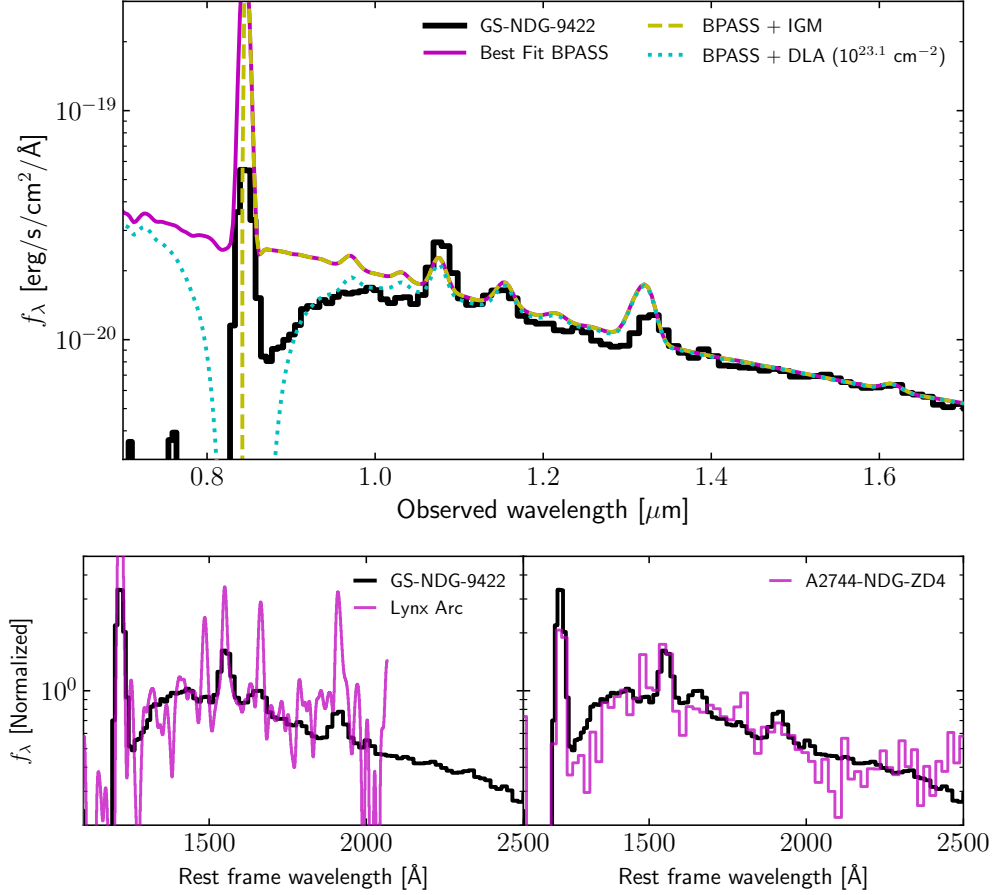


Fig. 2 *Top.* Zoom in on the rest-frame UV region of the JWST NIRSpec PRISM spectrum of GS-NDG-9422 (black) compared with the best fit models using a standard SSP (magenta) accounting for both the $z = 6$ IGM opacity (dashed yellow) and a DLA with column density of $10^{23.1} \text{ cm}^{-2}$ (dotted cyan). The full spectral fit for these models is shown in Methods. *Bottom.* Zoom in on the rest-frame UV region for GS-NDG-9422 (black) compared with the spectra of the $z = 3.35$ Lynx arc (left) and A2744-NDG-ZD4 at $z = 7.88$ (right). We have normalised the spectra and shifted them all to the rest frame.

Spectral fitting of GS-NDG-9422 with photoionization models (second panel of Figure 3) demonstrates that a blackbody model with $T = 10^{5.05} \text{ K}$ can provide a good fit to both the shape of the continuum and the majority of lower-ionization state emission line ratios. However, where our simple blackbody model fails is that it strongly *overpredicts* the flux of He II lines compared to those observed in the spectrum (bottom panels of Figure 3). The weak He II $\lambda 1640$ and He II $\lambda 4686$ in GS-NDG-9422 places tight constraints on the ionizing spectrum at $E > 4$ Rydberg. To explore this, we run models varying the leakage fraction of photons with $E > 4$ Rydberg from 0% (i.e. no He⁺-ionizing photons) to 100% (unattenuated blackbody). We conclude that

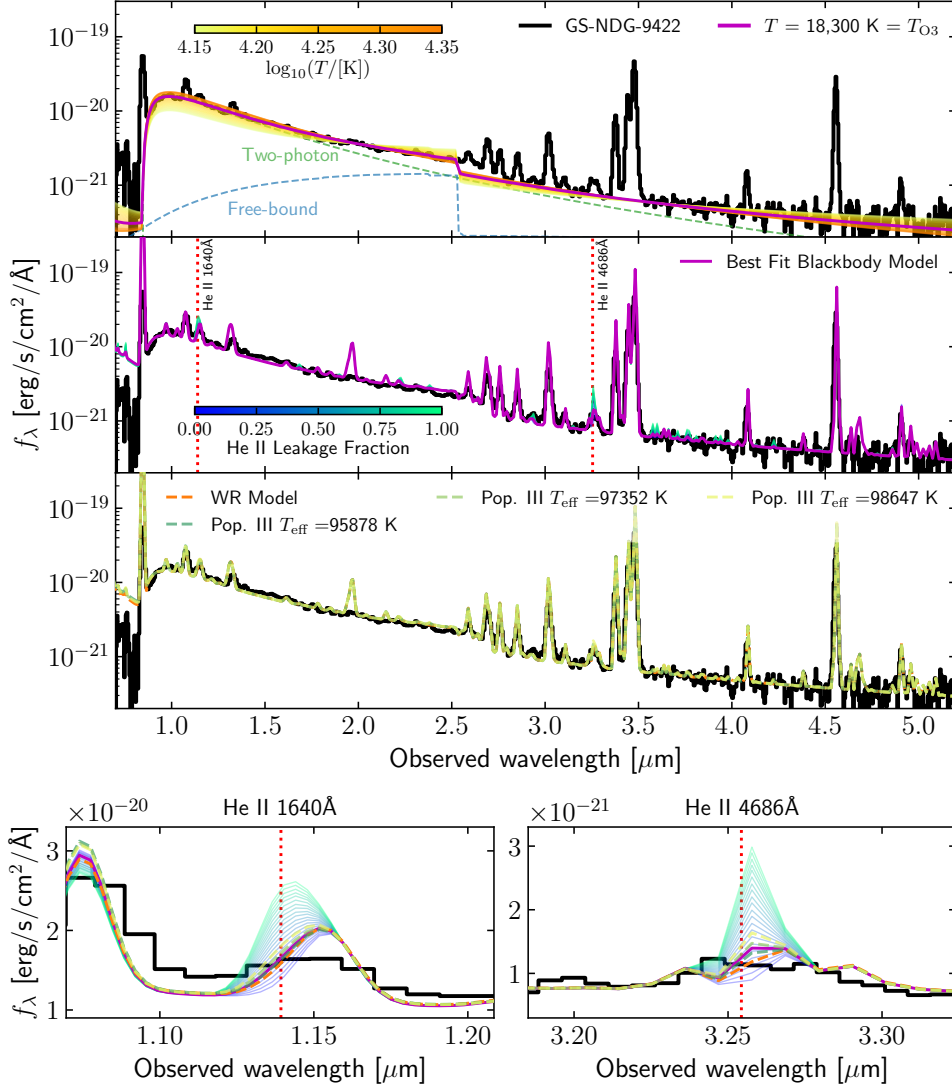


Fig. 3 *First Panel.* Predicted nebular continuum (coloured lines) for gas of primordial composition at fixed temperature (as listed in the colour bar and legend) compared to the JWST NIRSpec PRISM spectrum of GS-NDG-9422. The magenta line shows the prediction when using the gas temperature (T_{O3}) derived from the ratio of $[O\ III]\ \lambda 4363/\lambda 5007$, which nearly perfectly matches the continuum of the observed spectrum. *Second Panel.* Spectrum of GS-NDG-9422 (black) compared with the best fit blackbody model (magenta). The blue/green lines show the blackbody models with different leakage fractions of He II ionizing flux (see Methods). *Third Panel.* Spectrum of GS-NDG-9422 (black) compared with the Wolf-Rayet model with the most similar spectrum to the inferred SED (dashed orange) or various individual massive Pop. III stars with different effective temperatures (dotted lines). *Fourth Panel.* Zoom in on the regions around He II $\lambda 1640$ and He II $\lambda 1486$ demonstrating why the He II ionizing flux needs to be reduced in the blackbody models. Lines are the same as in the second and third panels.

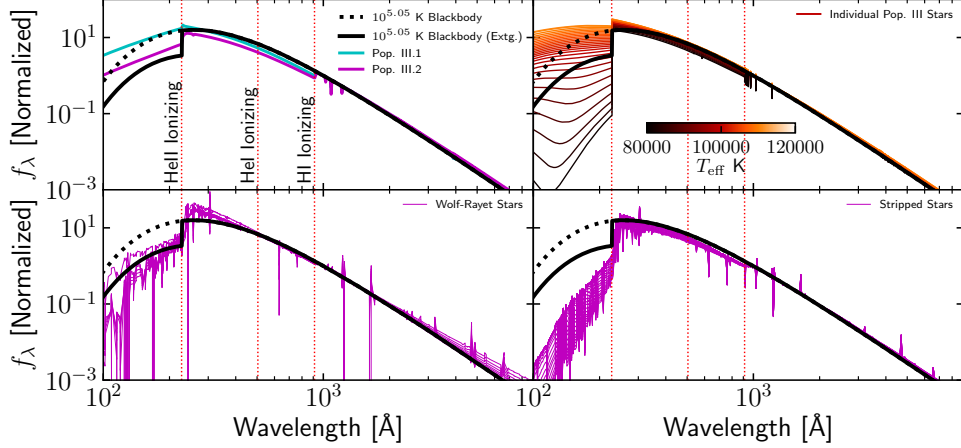


Fig. 4 Comparison of the best fit blackbody SED model (black) with the predicted spectra of Pop. III stars with varying IMFs (top left), individual massive Pop. III stars with different effective temperatures as shown in the colour bar (top right), low-metallicity Wolf-Rayet stars (bottom left), and stripped stars (bottom right). The dotted black line shows the blackbody spectrum prior to extinguishing the He II ionizing radiation.

75%–80% of the He^+ -ionizing photons emitted by the blackbody must be extinguished to match the observed He II emission (i.e. leakage fraction of $\lesssim 25\%$; Figure 4).

We note that other sources, including active galactic nuclei (AGN) or high-mass X-ray binaries (HMXBs), can have significant high-energy photon outputs, and have been invoked to explain peculiar emission line ratios seen at high-redshift [18, 19]. However, the weak He II emission disfavors power-law SEDs that extend past the He II ionizing edge. We exclude HMXBs due to the strong over-prediction of He II emission in these models (see Methods). Reproducing the observed spectrum with an AGN would require a peculiar absorption of the power-law spectrum [20]. Furthermore, the emission lines in GS-NDG-9422 do not show any evidence of a broad component that would be indicative of a broad-line region.

Massive metal-free Population III stars are predicted to have sufficiently high temperatures to power a two-photon dominated spectrum [10]. While the IMF of Population III stars is highly uncertain [21], comparing extremely top-heavy (Pop. III.1) and moderately top-heavy (Pop. III.2) Yggdrasil models [12] with our extinguished blackbody (Figure 4 top left) indicates these produce too many He^+ ionizing photons, while predictions for even less top-heavy IMFs begin to fall short of the required ξ_{ion} . In contrast, some individual Pop. III star models from [22] with effective temperatures of $\sim 97,000$ K and masses of $85 M_{\odot}$ to $108 M_{\odot}$ reasonably reproduce the required ionizing SED (Figure 4 top right). We note that the measured metallicity of $12 + \log_{10}(\text{O}/\text{H}) = 7.59 \pm 0.01$ suggests the presence of Pop. III stars is unlikely, unless we are witnessing the immediate enrichment and illumination of metals produced by primordial stars. Nevertheless, we consider these Pop. III star models in our analysis.

under the assumption that the atmospheres may be generally representative of hot massive stars at low metallicity.

Wolf-Rayet stars or stripped stars not only exhibit surface temperatures above 10^5 K, but can also have helium atmospheres that provide the necessary opacity to reduce their He^+ ionizing output. Compared to our best-fit extinguished blackbody, we find that stripped star SEDs [23] produce too few He^+ ionizing photons. However, select low-metallicity Wolf-Rayet models [24] show a remarkable resemblance (Figure 4).

We note that spectral fitting of some low-redshift reionization analogues has suggested a similar need for significant ionizing contribution from a hot ($T > 80,000$ K) blackbody [25], however the key difference in the high-redshift galaxies presented here is the dominance of the two-photon continuum. This necessitates an extremely high ξ_{ion} that cannot be produced if a substantial fraction of the ionizing photons are emitted by typical OB stars.

The progenitor masses of Wolf-Rayet stars at the metallicity of GS-NDG-9422 are not well constrained [26]. Masses of $\geq 37 M_{\odot}$ have been estimated for Wolf-Rayet stars in the Small Magellanic Cloud (SMC) with $T \gtrsim 100,000$ K [27], implying even higher progenitor masses. While this search may not be exhaustive, we conclude from Figure 4 that the nebular-dominated spectrum of GS-NDG-9422 is consistent with ionization powered by low-metallicity massive stars ($\gtrsim 50 M_{\odot}$), perhaps in the Wolf-Rayet phase.

Assuming a typical IMF, we expect to form one such $50 M_{\odot}$ star per $\sim 1,300 M_{\odot}$ of stellar mass. We repeat our photoionization modelling with our best-fit low-metallicity massive star and Wolf-Rayet models, maximizing the mass of an underlying stellar population with a normal IMF such that model spectrum remains a good fit (see Methods). For the two-photon continuum to remain dominant, we require $\leq 112 M_{\odot}$ of a normal stellar population per one low-metallicity massive star, or $\leq 137 M_{\odot}$ per one Wolf-Rayet star. This necessitates 35 times, or 9.5 times, more massive stars compared to a typical IMF in the low-metallicity massive star scenario, or Wolf-Rayet star scenario, respectively (Methods). Either scenario implies that the IMF in GS-NDG-9422 must be extraordinarily top-heavy.

The IMF is predicted to get progressively more top-heavy for low-metallicity gas at high pressure [2, 3], and a top-heavy IMF has been suggested to explain IR emission line ratios [28] and the surprising abundance of UV-bright galaxies [29] observed at high redshift.

The strong contribution of the two-photon continuum to the overall spectrum of GS-NDG-9422 demonstrates the need to update SED fitting templates to account for stellar populations with extreme ξ_{ion} . The intrinsic ξ_{ion} for our best-fit blackbody model is 26.4 Hz erg^{-1} , $10\times$ greater than commonly adopted for star-forming galaxies in reionization models [30]. Since our modelling indicates that GS-NDG-9422 has an ionizing escape fraction of 7.3%, significantly fewer nebular dominated galaxies (NDGs) are required to drive reionization compared to star-forming galaxies, motivating future work to constrain their number density and luminosity function.

The striking similarities between GS-NDG-9422 and both the Lynx arc and A2744-NDG-ZD4 suggest that NDGs powered by a very top-heavy IMF may not be rare at high redshift. Selecting NDGs at high redshift when the IGM is opaque to $\text{Ly}\alpha$

will be challenging because without $\text{Ly}\alpha$, the two-photon UV turnover is degenerate with a DLA. Nevertheless, the exotic nature of GS-NDG-9422 and A2744-NDG-ZD4 demonstrate that our understanding of star formation in the early Universe requires substantial revision.

1 Methods

1.1 Data

GS-NDG-9422 was observed in the JADES survey (PID: 1210, PI: Luetzendorf) in five spectral modes, receiving 28 hours integration in Prism/CLEAR and 7 hours integration in each of G140M/F070LP, G235/F170LP, G395M/F290LP and G395H/F290LP. We use the reduced spectra released as part of the JADES Public Data Release [31, 32].

A2744-NDG-ZD4 was observed as part of the Ultra-deep NIRC2 and NIRS2 Observations Before the Epoch of Reionization (UNCOVER) program (ID: 2561, PI: Labbe; [33]) in the lensing field Abell 2744. A2744-NDG-ZD4 is lensed with magnification factor of $\mu = 1.96$ [34], and received 2.3 hours integration in Prism/CLEAR. Reduced data was retrieved from the Dawn JWST Archive (DJA)¹. The data was reduced using the custom-made pipeline MsaExp v.0.6.12². Further details of the reduction pipeline are given in [35].

The spectrum of the Lynx arc was taken with the Keck I telescope using the Low Resolution Imaging Spectrograph (LRIS) [15].

1.2 Emission line fitting

Where possible, emission lines were fit with a single component Gaussian profile with the continuum modelled as a 1D spline. In cases where lines are sufficiently blended we fit the whole complex with one component. In some cases, partially blended lines are fit simultaneously with neighbouring lines and fluxes reported separately. These are marked in Table 2. We fit all identifiable lines and report upper limits for notable undetected lines.

Line fluxes from higher resolution grating spectra of GS-NDG-9422 were measured independently. Fluxes derived from different observations are mildly discrepant in some cases. Notably, $\text{H}\beta$, $[\text{OIII}] \lambda 4959$, $[\text{OIII}] \lambda 5007$ and $\text{H}\alpha$ lines exhibit higher fluxes in the grating modes. This behaviour is reported in [32] who suggest that the Prism flux calibration is more reliable. We note that in low-resolution data, the continuum level for some emission lines can be ambiguous, especially for $\text{Ly}\alpha$, $\text{He II} + \text{O III}]$ and $[\text{O II}]$, which introduces uncertainty into the emission lines flux. Throughout our analysis, we adopt the Prism fluxes where possible. However, we ensure that conclusions presented in this work are generally consistent with the measured grating fluxes. Emission lines in the high-resolution grating show no evidence of a broad component and are well fit with a single component with velocity dispersions $< 200 \text{ km s}^{-1}$.

¹<https://dawn-cph.github.io/dja/index.html>

²<https://zenodo.org/record/8319596>

	Prism/CLEAR	G140M	G235M	G395M	G395H
Ly- α	110.1 \pm 2.8	101.4 \pm 4.3
Nv λ 1239		< 5.4
Nv λ 1243		< 4.9
Niv] λ 1483		< 2.4
Niv] λ 1486		< 3.1
Civ λ 1548		21.5 \pm 1.1 [†]
Civ λ 1550		17.6 \pm 1.1 [†]
Civ $\lambda\lambda$ 1549	37.8 \pm 0.9				
HeII λ 1640		5.1 \pm 0.9
OIII] λ 1660		< 2.5 [†]
OIII] λ 1666		4.9 \pm 1.0 [†]
HeII+OIII]	15.1 \pm 1.1				
NIII] $\lambda\lambda$ 1750		< 1.9
CIII] $\lambda\lambda$ 1909	13.6 \pm 0.9	8.0 \pm 1.0
[OII] $\lambda\lambda$ 3727	2.2 \pm 0.2	...	3.0 \pm 0.6
H11	< 1.0
H10	< 0.8
H9	1.2 \pm 0.3
[NeIII] λ 3869		...	6.2 \pm 0.5
HeI λ 3889		...	1.6 \pm 0.4
[NeIII]+HeI	7.6 \pm 0.4				
H δ	4.3 \pm 0.5
H γ	8.3 \pm 0.4 [†]	...	7.5 \pm 0.5	8.1 \pm 0.5	5.9 \pm 0.6
[OIII] λ 4363	2.8 \pm 0.4 [†]	...	2.6 \pm 0.7	3.4 \pm 0.5	2.8 \pm 0.5
HeI λ 4471	0.8 \pm 0.1	...	< 3.1	< 14.6	2.1 \pm 0.5
HeII λ 4686	1.1 \pm 0.2 [†]	< 1.5	< 2.4
[ArIV] λ 4711 [‡]	0.8 \pm 0.2 [†]	1.5 \pm 0.4	< 1.3
[ArIV] λ 4740	0.4 \pm 0.2 [†]	< 0.8	< 1.2
H β	17.2 \pm 0.3	19.4 \pm 0.5	19.6 \pm 0.5
[OIII] λ 4959	32.3 \pm 0.4	36.3 \pm 0.7	36.4 \pm 0.6
[OIII] λ 5007	97.1 \pm 0.8	102.2 \pm 1.1	98.7 \pm 1.5
HeI λ 5875	2.2 \pm 0.1	1.3 \pm 0.4	...
[OI] λ 6300	< 0.5	< 1.7	< 1.3
H α	45.5 \pm 0.6	52.5 \pm 0.9
[NII] λ 6583	< 1.4
[SII] λ 6716	< 0.5	< 1.6
[SII] λ 6731	< 0.5	< 1.7
HeI λ 7065	1.2 \pm 0.1	< 2.9	< 2.1

Table 1 Emission line flux measurements for GS-NDG-9422 across each observed spectrum. Fluxes are reported in units of $\times 10^{-19}$ erg s $^{-1}$ cm $^{-2}$.

[†] Fit simultaneously with neighbouring line and fluxes reported separately.

[‡] Blended with He I λ 4713.

1.3 Calculation of physical conditions

Throughout this section, we make use of PYNEB [36] using atomic data from CHIANTI (version 10.0.2; [37, 38]).

Dust extinction

Balmer decrements H δ /H β and H γ /H β from the Prism and H9/H β from the grating are consistent with Case B values, indicating that there is no significant dust reddening in GS-NDG-9422 (Figure 5). Measured H α /H β ratios are lower than theoretically predicted at $T = 10^4$ K. Note, this is not suggestive of dust reddening, since this would

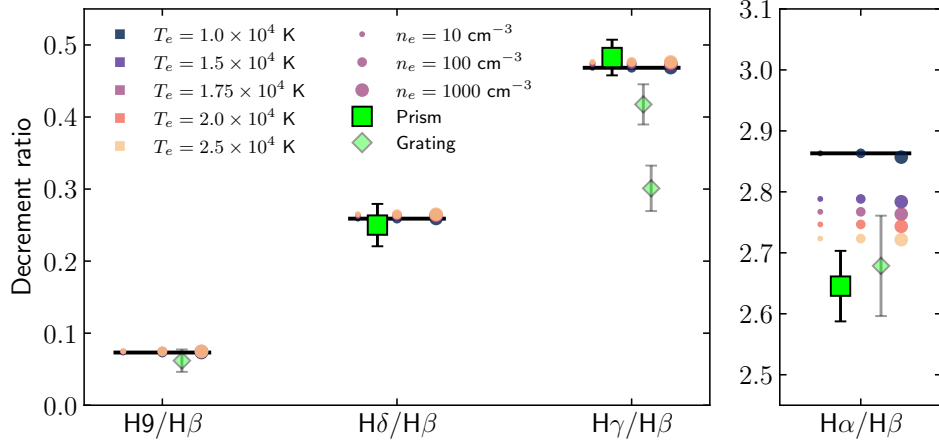


Fig. 5 Observed Balmer decrement ratios compared to theoretical values at different temperatures and densities. Green squares give the measured ratios from the Prism, while diamonds give ratios measured from gratings, where available. Solid black lines give the theoretical ratio for case B recombination at $T_e = 10^4$ K and $n_e = 100 \text{ cm}^{-3}$. Coloured points show theoretical ratios for a range of temperatures ($10^4 \leq T_e \leq 2.5 \times 10^4$ K; color) and densities ($n_e = 10, 100, 1000 \text{ cm}^{-3}$; marker size).

act in the opposite direction. At higher temperatures, the theoretical ratio decreases, and our G395H/F290LP measurement is consistent with theoretical ratios with $T_e \gtrsim 2 \times 10^4$ K, possibly indicative of a very hot nebula. $\text{H}\gamma/\text{H}\beta$ measured from the medium-resolution grating is marginally below the theoretical value. In isolation, this could suggest non-zero dust reddening; however, this evidence is outweighed by the other measured ratios. The high-resolution grating returns a much lower $\text{H}\gamma/\text{H}\beta = 0.3 \pm 0.03$. However, we note that the continuum is undetected in the high-resolution grating, which contributes uncertainty to the measured ratio. Note that much of the focus of this work is the unusually strong two-photon nebular continuum at $\lambda_{\text{rest}} \approx 1400 \text{ \AA}$. If there is significant dust in this system, the intrinsic two-photon continuum would be even higher than measured here, requiring more extreme scenarios than those discussed in this work.

Electron temperature

The temperature-sensitive $[\text{O III}] \lambda 4363/\lambda 5007$ ratio can be measured from each of the Prism, G395M and G395H observations, yielding three consistent independent temperature measurements ($T_e = 1.83 \pm 0.15, 1.99 \pm 0.18$, and $1.81 \pm 0.18 \times 10^4$ K, respectively). The temperature derived from the medium-resolution $[\text{O III}] \lambda 1666/\lambda 5007$ ratio is somewhat lower ($T_e = 1.70^{+0.05}_{-0.06} \times 10^4$ K). However, the $\text{He II} + [\text{O III}]$ flux measured from the medium-resolution grating is significantly lower than that of the Prism. Instead, the measured temperature from above ($T_e = 1.83 \times 10^4$ K) implies $\lambda\lambda 1660, 1666/\lambda 5007 = 0.08$, which gives $f_{\lambda\lambda 1660, 1666} = 8.2 \pm 0.1 \times 10^{-19} \text{ erg s}^{-1} \text{ cm}^{-2}$ based on the $[\text{O III}] \lambda 5007$ Prism flux, consistent with $[\text{O III}]$ contributing $\sim 55\%$ of

Property	Derived value
$T_e(\text{O}^{++})$	$18,300 \pm 1,500 \text{ K}$
n_e	$\lesssim 10^3 \text{ cm}^{-3}$
$12 + \log(\text{O}^{++}/\text{H}^+)$	7.58 ± 0.01
$12 + \log(\text{O}^+/\text{H}^+)$	$5.79^{+0.04}_{-0.03}$
$12 + \log(\text{O}/\text{H})$	7.59 ± 0.01
$\log(\text{N}^{++}/\text{O}^{++})$	< -0.85
$\log(\text{C}^{++}/\text{O}^{++})$	-0.76 ± 0.03
$\log(\text{C}/\text{O})$	-0.73 ± 0.03
$\log(\text{Ne}/\text{O})$	$-0.85^{+0.03}_{-0.04}$
He^+/H^+	0.10 ± 0.01
$\text{He}^{++}/\text{H}^+$	0.005 ± 0.001
He/H	0.11 ± 0.01
$\log(\text{O}^{++}/\text{O}^+)$	$1.79^{+0.03}_{-0.04}$
$\text{He}^{++}/\text{He}^+$	0.06 ± 0.01

Table 2 Physical properties and chemical abundances derived for GS-NDG-9422.

the measured Prism He II+O III] blend. The implied He II $\lambda 1640$ flux ($6.9 \pm 1.1 \times 10^{-19} \text{ erg s}^{-1} \text{ cm}^{-2}$) is consistent with that expected by extrapolating from $f_{\lambda 4686}$ using the theoretical He II $\lambda 1640/\lambda 4686$ ratio. Note that this further supports the conclusion of a lack of dust in this system since the He II $\lambda 1640$ would be subject to extremely high extinction, relative to the $\lambda 4686$ line. The magnitude of the Balmer jump is sensitive to T_e (e.g. [6, 39]). In Figure 3, we show this behaviour for model nebular continuum spectra for a range of temperatures, finding that the Balmer jump magnitude and two-photon continuum contribution are fully consistent with $T_e = 1.83 \pm 0.15 \times 10^4 \text{ K}$, as derived from [O III].

Electron density

The detection of the two-photon nebular continuum implies $n_e \lesssim 10^3 \text{ cm}^{-3}$ since this feature is strongly suppressed by l -changing collisions at higher densities (Figure 8). The density-sensitive doublets of C III] and [O II] are not resolved in our observations, while N IV] and [S II] are not detected. We report a marginal detection of the [Ar IV] $\lambda\lambda 4711, 4740$ doublet in the Prism spectrum. These lines are partially blended with each other and He II $\lambda 4686$, while [Ar IV] $\lambda 4711$ is also completely blended with He I $\lambda 4713$. Our three-component fit to this complex yields [Ar IV] $\lambda 4711/\lambda 4740 = 1.6 \pm 0.8$ after subtracting the predicted He I $\lambda 4713$ contribution (assuming $\lambda 4713/\lambda 4471 = 0.15$), consistent with the low-density limit ($n_e \lesssim 10^4 \text{ cm}^{-3}$).

Chemical abundances

We derive chemical abundances for GS-NDG-9422 adopting $T_e = 1.83 \times 10^4 \text{ K}$ and a density of $n_e = 100 \text{ cm}^{-3}$ following the procedure in [40]. Given the apparent agreement between $T_e(\text{H}^+)$ and $T_e(\text{O}^{++})$, we assume a constant temperature for all ionisation zones, deriving $12 + \log(\text{O}/\text{H}) = 7.59 \pm 0.01$ with both Prism and grating line fluxes. We derive the carbon abundance from the C III] $\lambda\lambda 1907, 1909$ / [O III] $\lambda 5007$ ratio measured from the Prism, assuming no dust, finding $\log(\text{C}/\text{O}) = -0.73 \pm 0.03$ after applying the ionisation correction factor presented in [41]. However, we note the

significant emission from C IV in the spectrum. Given the high ξ_{ion} implied for GS-NDG-9422, the ICF may not be representative of the conditions in GS-NDG-9422 (e.g. [42]), and the quoted C/O may represent a lower limit.

Since no nitrogen lines are detected in GS-NDG-9422, we can only place upper limits on the nitrogen abundances. The low O^+ abundance implies that the N^+ abundance is likely negligible. We instead consider the N^{++} abundance using $\text{N III}] \lambda\lambda 1750 / [\text{O III}] \lambda 5007$ measured from the Prism, and $\text{N III}] \lambda\lambda 1750 / \text{O III}] \lambda 1666$ measured from the grating. These yield $3\text{-}\sigma$ upper limits of $\log(\text{N}^{++}/\text{O}^{++}) < -0.85$ and < -1.01 respectively. We adopt the former as our preferred limit.

We detect several helium recombination lines from both the singly and doubly ionised states. Prism measurements of $\text{He I } \lambda 4471 / \text{H}\beta$ and $\text{He I } \lambda 5875 / \text{H}\beta$ yield consistent measurements of $\text{He}^+/\text{H}^+ = 0.10 \pm 0.005$ and 0.10 ± 0.01 respectively. Deriving a $\text{He}^{++}/\text{H}^+$ abundance using the $\text{He II } \lambda 4686$ line results in only a $6 \pm 1\%$ contribution to the total helium abundance, giving $\text{He}^{++}/\text{H}^+ = 0.005 \pm 0.001$. Together, this implies a total helium abundance of $\text{He}/\text{H} = 0.11 \pm 0.01$, higher than typical values observed in low-metallicity systems [43], but consistent with some massive globular clusters [44]. However, we caution that our derived helium abundance does not account for collisional emission or self-absorption, which could be significant (e.g. [45]).

1.4 DLA with a Contrived Geometry

We consider what kind of DLA geometry can reproduce the spectral shape of GS-NDG-9422 and A2744-NDG-ZD4. For GS-NDG-9422, we use the best fit BPASS model (see below) and apply damping due to a foreground DLA with leakage through optically-thin channels. A similar approach is applied to A2744-NDG-ZD4; however, due to the lower signal-to-noise, we apply a power-law fit to the spectrum to represent the intrinsic stellar continuum. In the top panel of Figure 6 we show the fits to both galaxies, and demonstrate that they require column densities $> 10^{23.3} \text{ cm}^{-2}$ and a covering fraction of 70%. Not only would these DLAs be the highest neutral columns observed (see bottom panel of Figure 6), they must also have optically thin channels covering 30% of the total area. Furthermore, at these column densities, the gas can self-shield from the local-radiation field, and the core would be expected to be fully molecular. Given the fine-tuned requirements, we consider this scenario of a thick DLA with holes highly unlikely.

1.5 Spectral Modelling

Spectral modelling is performed using the photoionization code CLOUDY v23 [49].

Nebular continuum as a function of temperature

To calculate the nebular continuum in the top panel of Figure 3, we set up a spherical shell of gas with primordial composition in CLOUDY and irradiate it with two “lasers” with energies just above that needed to ionize hydrogen and singly ionize helium. The gas temperature is varied in the range $10^{4.15} \leq T/\text{K} \leq 10^{4.35}$.

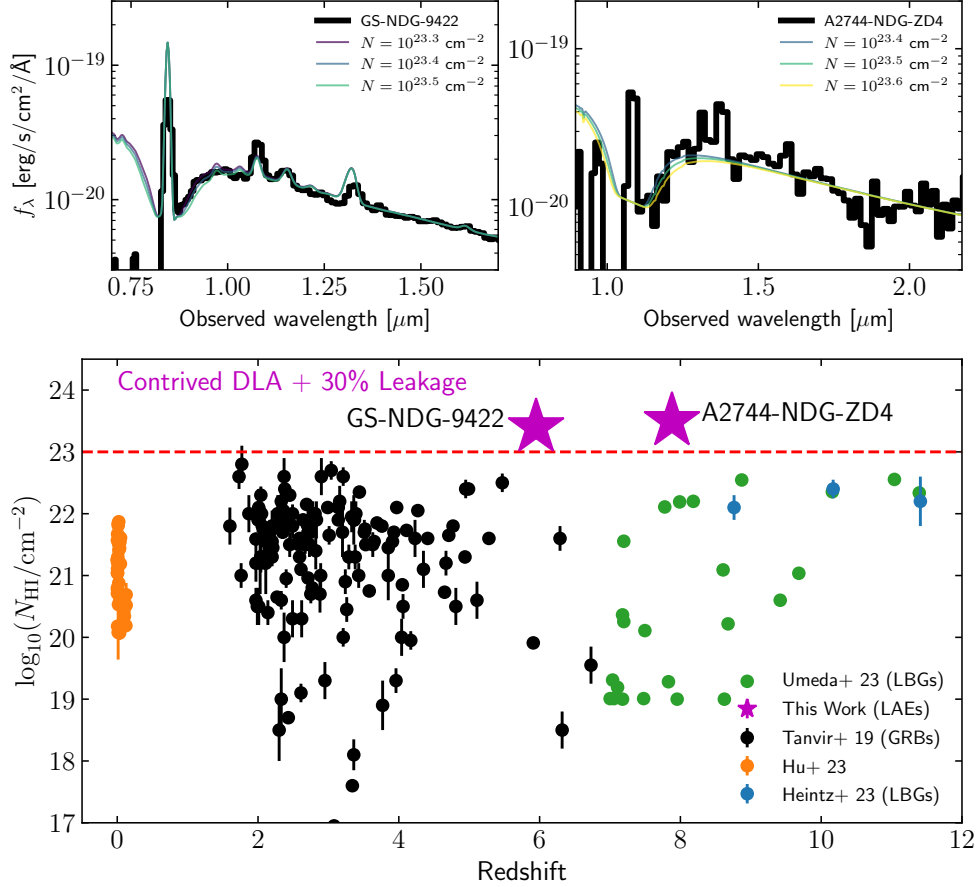


Fig. 6 *Top.* Fits to GS-NDG-9422 and A2744-NDG-ZD4 using a DLA model with a 70% covering fraction. *Bottom.* Comparison of the required DLA column density with low-redshift star-bursting galaxies (orange, [46]), intermediate redshift GRBs (black, [47]), and high-redshift JWST galaxies (blue, green, [35, 48]), as well as the galaxies presented in this work (magenta), that also require a $< 100\%$ DLA covering fraction.

Models with standard SSPs

We adopt the BPASS v2.2.1 SSP models including binary stellar evolution [50] with a maximum mass of $300 M_{\odot}$ and a high-mass slope of -2.35 . We consider a population with an age of 3 Myr and a metallicity of $0.1 Z_{\odot}$, consistent with that measured for the gas from the spectrum. We adopt a spherical geometry with an inner radius of 0.1 pc. The calculation is stopped at an electron fraction of 1% or when the neutral column density reaches $10^{18.7} \text{ cm}^{-2}$, consistent with the minimal observed Ly α emission offset ($\lesssim 100 \text{ km s}^{-1}$) [51]. We vary gas density, ionization parameter, metallicity (assuming solar abundance patterns from [52]), and carbon abundance. The gas temperature is fixed to that measured from [O III] $\lambda 4363/\lambda 5007$. The best fit model ($n = 10^3 \text{ cm}^{-3}$,

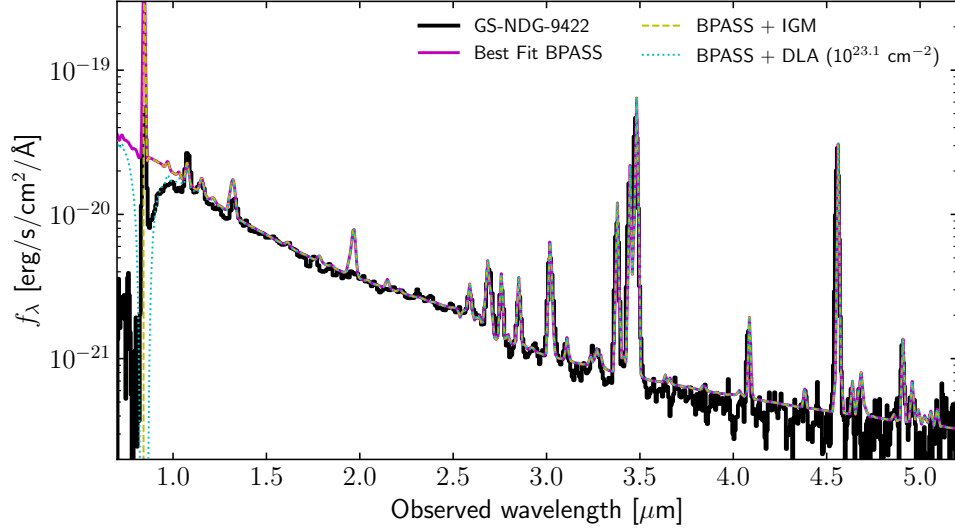


Fig. 7 JWST NIRSpec PRISM spectrum of GS-NDG-9422 (black) compared with the best fit models using a standard SSP (magenta) accounting for both the $z = 6$ IGM opacity (dashed yellow) and a DLA with column density of $10^{23.1} \text{ cm}^{-2}$ (dotted cyan).

$\log_{10}(U) = 1.2$, $\log_{10}(Z_{\text{O}}/Z_{\odot}) = -1.1$, and $\log_{10}(Z_{\text{C}}/Z_{\odot}) = -1.4$; Figure 2 & 7) is obtained matching the line strengths of [O III] $\lambda 5007$, [O II] $\lambda \lambda 3727$, C III] $\lambda \lambda 1909$, H α , and H γ with respect to H β , meaning the resulting continuum is a prediction of the model. Assuming $z = 6$ IGM transmission curves from [53], we find that IGM damping is unable to produce the observed UV turnover from this BPASS model (yellow dashed line in Figure 2). Even the maximal IGM damping wing, calculated following the formalism presented in [13, 54], cannot reproduce this feature. Similar results were found in [14] at much higher redshift. We model damping due to the presence of a DLA with CLOUDY by calculating the transmission of the best-fit model through slabs of neutral hydrogen with varying column densities (best fit shown as dotted blue line in Figure 2 & 7).

Models with blackbodies

The CLOUDY setup for our models with blackbody SEDs are nearly identical to those with SSPs. To gain insight into the requirements for the two-photon continuum to dominate over the ionizing SED, we initialize hydrogen-only gas at constant temperature (measured from [O III] $\lambda 4363/\lambda 5007$) and systematically vary the density and blackbody temperature (Figure 8). A weak UV turnover begins to appear at temperatures $\gtrsim 65,000 \text{ K}$, which is hotter than a typical O star. A strong UV turnover requires at least $T \gtrsim 90,000 \text{ K}$. The two-photon continuum is also sensitive to gas density because, at high densities, l -changing collisions will suppress the two-photon emission relative to Ly α . This is seen in the bottom panel of Figure 8 where we vary gas density for a fixed blackbody temperature of $100,000 \text{ K}$. The UV turnover

Parameter	Value
n	10^3 cm^{-3}
T_{BB}	$10^{5.05} \text{ K}$
U	0.0
T_{gas}	$10^{4.3} \text{ K}$
Z_{O}/Z_{\odot}	-1.1
Z_{C}/Z_{\odot}	-1.6
O32	37.1
He II leakage	0.22

Table 3 Parameters for the optimized blackbody model.

is strongly suppressed at $n \gtrsim 10^3 \text{ cm}^{-3}$. We emphasize that the details of this calculation are sensitive to the chosen column density at which the model is truncated (which in our case is set by the velocity offset of $\text{Ly}\alpha$). Furthermore, there exist significant differences in atomic data predictions for the strength of l -changing collisions as a function of temperature [55].

To optimize the blackbody model fit to GS-NDG-9422, we begin with the parameters of the best fit BPASS model and update ionization parameter, gas density, and blackbody temperature to simultaneously reproduce the emission line ratios and continuum shape. We allow for both density and ionization bounded nebulae by adding an additional stopping criteria to reproduce the measured $[\text{O II}] \lambda\lambda 3727/[\text{O III}] \lambda 5007$ (O32) ratio. This stopping criteria often supersedes the neutral gas column stopping criteria used above. The O32 ratio and the gas temperature are allowed to vary within their observational uncertainties. As a final step, we add an additional parameter to extinguish the ionizing flux at $E > 4$ Rydberg to control the strength of the He II emission, varying the leakage fraction of He II-ionizing photons from the blackbody between 0 and 1 (coloured lines in second panel of Figure 3). The parameters for our optimized model are reported in Table 3. We note that all our models predict strong Mg II $\lambda 2796, 2803$ emission at $\lambda_{\text{obs}} \approx 1.95 \mu\text{m}$. Since this doublet is resonant and $f_{\text{esc}}(\text{Ly}\alpha) \ll 100\%$, this feature is likely to be strongly suppressed. Alternatively, its absence in GS-NDG-9422 could simply indicate sub-solar Mg/O [56].

Models with Wolf-Rayet stars

Adopting parameters from the optimised blackbody model but removing the He II leakage parameter, we replaced the blackbody SED with a theoretical low-metallicity Wolf-Rayet star spectrum. We consider the WNL-H40 grid of the PoWR Wolf-Rayet models [24] with $Z = 0.07 Z_{\odot}$, similar to that derived for GS-NDG-9422. We identify model 13-10 as most similar to our optimised blackbody, with $T = 100,000 \text{ K}$ and $L = 10^{5.3} L_{\odot}$. No further optimisation is performed and the resulting spectrum is shown as the dashed orange line in Figure 3, nearly identical to the optimised blackbody model.

Models with individual Population III stars

We repeat the exercise described for our Wolf-Rayet models, this time replacing the blackbody SED with three Pop. III star models from [22] with effective temperatures between 95,000 K and 99,000 K.

Models with high-mass X-ray binaries stars

Following [19, 57], we model the X-ray sources using a modified blackbody spectrum [58]. We assume black hole masses in the range $6 - 25 M_{\odot}$ and disk radii between $10^3 - 10^4$ gravitational radii. In order for a UV turnover to appear, the ionizing photon output from the XRBs must dominate over the stellar population so that the nebular continuum can outshine the stars, implying a very high ratio of X-ray luminosity to star formation rate. In Figure 9, we show our XRB model for $25 M_{\odot}$ black holes optimised to reproduce the continuum shape of GS-NDG-9422. This model significantly overpredicts the strength of the He II $\lambda 1640$ and $\lambda 4686$ lines. Varying the black hole masses does not resolve this issue. We therefore conclude that XRBs are not the dominant ionizing source in GS-NDG-9422.

On the lack of Wolf-Rayet wind features

Although Wolf-Rayet stars are typically associated with broad emission lines due to their high-velocity stellar winds, the absence of these features in GS-NDG-9422 could simply be the result of the extremely bright nebular component outshining these wind features, as predicted by our photoionization models. Furthermore, in the absence of iron, which is the dominant source of stellar atmospheric opacity, wind speeds can drop below 500 km s^{-1} , even at solar oxygen abundance [59]. Hence, high-redshift Wolf-Rayet dominated galaxies may not show broad He II $\lambda 1640$ and He II $\lambda 4686$ lines [60].

Ionizing flux required to power $H\beta$

The hydrogen ionizing photon luminosity, Q , can be measured from the $H\beta$ flux as:

$$Q \approx \frac{4\pi D_l^2 I_{H\beta}}{(1 - f_{\text{esc}})h\nu_{H\beta}} \frac{\alpha_B}{\alpha_B^{\text{eff}}}, \quad (1)$$

Where $D_l = 58456.2 \text{ Mpc}$ is the luminosity distance, $I_{H\beta}$ is the measured $H\beta$ flux, h is Planck's constant, $\nu_{H\beta}$ is the frequency of the $H\beta$ transition, α_B is the total case B recombination rate, f_{esc} is the escape fraction of ionizing photons, and α_B^{eff} is the effective $H\beta$ recombination rate. To calculate a luminosity distance, we adopt a cosmology with $H_0 = 67.31 \text{ km s}^{-1} \text{ Mpc}^{-1}$ and $\Omega_m = 0.315$ [61]. The escape fraction is derived from our best fitting blackbody photoionization model to be 7.3% and the recombination rates are evaluated at 20,000 K [62].

IMF excess

To calculate the excess number of massive stars we re-run our best Wolf-Rayet model and the low-metallicity massive star model with $T_{\text{eff}} = 97,352 \text{ K}$ while simultaneously adding a second component BPASS model. In the case of low-metallicity massive stars, we assume the BPASS model has an age of 3 Myr (the approximate lifetime of massive stars), while for the Wolf-Rayet models, we assume the progenitor stars are lower mass ($50 M_{\odot}$) and live for slightly longer (5 Myr). We assume the BPASS stellar population has the same metallicity as the gas. We then progressively increase the

ionization parameter of the second population until the UV turnover from the two-photon continuum begins to weaken. We calculate the stellar mass of a BPASS SSP that can be present per hot star as

$$M_{\text{SSP}} = \frac{U_{\text{SSP}}}{U_{\text{star}}} \frac{Q_{\text{star}}}{Q_{\text{SSP}}}, \quad (2)$$

where $Q_{\text{star}} = 10^{49.36} \gamma \text{ s}^{-1}$ for Wolf-Rayet stars or $10^{49.98} \gamma \text{ s}^{-1}$ for low-metallicity massive stars with $T_{\text{eff}} = 97,352 \text{ K}$. $Q_{\text{SSP}} = 10^{46.73}$ or $10^{46.03} \gamma \text{ s}^{-1} \text{ M}_{\odot}^{-1}$ at 3 Myr and 5 Myr, respectively. In both cases $\frac{U_{\text{SSP}}}{U_{\text{star}}} = 6.3\%$. Therefore, $M_{\text{SSP}} = 112$ or 137 M_{\odot} for low-metallicity massive stars and Wolf-Rayet stars, respectively. Based on a BPASS SSP of 112 M_{\odot} , one would expect on average 0.029 stars of $> 100 \text{ M}_{\odot}$ while for an SSP of 137 M_{\odot} , the expectation is 0.105 stars of $> 50 \text{ M}_{\odot}$. In other words, there is a $35\times$ excess in the number of massive stars in the case of our low-metallicity massive star model, or a $9.5\times$ excess for our Wolf-Rayet model.

The results of this calculation are sensitive to the chosen underlying SSP, the progenitor masses of Wolf-Rayet stars, and the mass of the low-metallicity massive stars. For SSPs that have intrinsically lower ξ_{ion} , the excess drops as Q_{SSP} appears in the denominator of Figure 2. If the ages at which the exotic stars evolve off the main sequence is longer than what we have assumed here, the excess will also decrease. Nevertheless, we highlight that the excess number of massive stars we have calculated represents a conservative lower limit because we have maximized the allowable contribution from the SSP in the model.

These values allow us to calculate the maximum mass of the star clusters that formed in GS-NDG-9422. Calculating the number of stars based on the $\text{H}\beta$ luminosity, GS-NDG-9422 would be powered by $\sim 17,000$ very metal-poor stars of $\sim 100 \text{ M}_{\odot}$ with $T_{\text{eff}} = 97,000 \text{ K}$, or $\sim 70,000$ low-metallicity Wolf-Rayet stars. Based on the above calculations, this implies a maximum star cluster mass of $10^{6.55} \text{ M}_{\odot}$ or $10^{7.12} \text{ M}_{\odot}$ for the low-metallicity massive star or Wolf-Rayet star cases, respectively.

Acknowledgments. We thank Bob Fosbury for useful discussions and providing us with the LRIS spectrum of the Lynx arc. We thank Thibault Garel for providing us with the simulated IGM attenuated curves from the SPHINX simulation. AJC, AS and AJB, acknowledge funding from the “FirstGalaxies” Advanced Grant from the European Research Council (ERC) under the European Union’s Horizon 2020 research and innovation programme (Grant agreement No. 789056). CW thanks the Science and Technology Facilities Council (STFC) for a PhD studentship, funded by UKRI grant 2602262. NL acknowledges support from the Kavli foundation. HK acknowledges support from the Beecroft Fellowship.

References

- [1] Bastian, N., Covey, K.R., Meyer, M.R.: A Universal Stellar Initial Mass Function? A Critical Look at Variations. *ARA&A* **48**, 339–389 (2010) <https://doi.org/10.1146/annurev-astro-082708-101642> [arXiv:1001.2965](https://arxiv.org/abs/1001.2965) [astro-ph.GA]

- [2] Chon, S., Omukai, K., Schneider, R.: Transition of the initial mass function in the metal-poor environments. *MNRAS* **508**(3), 4175–4192 (2021) <https://doi.org/10.1093/mnras/stab2497> [arXiv:2103.04997](https://arxiv.org/abs/2103.04997) [astro-ph.GA]
- [3] Sneppen, A., Steinhardt, C.L., Hensley, H., Jermyn, A.S., Mostafa, B., Weaver, J.R.: Implications of a Temperature-dependent Initial Mass Function. I. Photometric Template Fitting. *ApJ* **931**(1), 57 (2022) <https://doi.org/10.3847/1538-4357/ac695e> [arXiv:2205.11536](https://arxiv.org/abs/2205.11536) [astro-ph.GA]
- [4] Saxena, A., Bunker, A.J., Jones, G.C., Stark, D.P., Cameron, A.J., Witstok, J., Arribas, S., Baker, W.M., Baum, S., Bhatawdekar, R., Bowler, R., Boyett, K., Carniani, S., Charlot, S., Chevallard, J., Curti, M., Curtis-Lake, E., Eisenstein, D.J., Endsley, R., Hainline, K., Helton, J.M., Johnson, B.D., Kumari, N., Looser, T.J., Maiolino, R., Rieke, M., Rix, H.-W., Robertson, B.E., Sandles, L., Simmonds, C., Smit, R., Tacchella, S., Williams, C.C., Willmer, C.N.A., Willott, C.: JADES: The production and escape of ionizing photons from faint Lyman-alpha emitters in the epoch of reionization. *arXiv e-prints*, 2306–04536 (2023) <https://doi.org/10.48550/arXiv.2306.04536> [arXiv:2306.04536](https://arxiv.org/abs/2306.04536) [astro-ph.GA]
- [5] Peimbert, M., Costero, R.: Chemical Abundances in Galactic HII Regions. *Boletín de los Observatorios Tonantzintla y Tacubaya* **5**, 3–22 (1969)
- [6] Guseva, N.G., Izotov, Y.I., Thuan, T.X.: Balmer and Paschen Jump Temperature Determinations in Low-Metallicity Emission-Line Galaxies. *ApJ* **644**(2), 890–906 (2006) <https://doi.org/10.1086/503865> [arXiv:astro-ph/0603134](https://arxiv.org/abs/astro-ph/0603134) [astro-ph]
- [7] Katz, H., Rosdahl, J., Kimm, T., Blaizot, J., Choustikov, N., Farcy, M., Garel, T., Haehnelt, M.G., Michel-Dansac, L., Ocvirk, P.: The Sphinx Public Data Release: Forward Modelling High-Redshift JWST Observations with Cosmological Radiation Hydrodynamics Simulations. *arXiv e-prints*, 2309–03269 (2023) <https://doi.org/10.48550/arXiv.2309.03269> [arXiv:2309.03269](https://arxiv.org/abs/2309.03269) [astro-ph.GA]
- [8] Endsley, R., Stark, D.P., Whitler, L., Topping, M.W., Johnson, B.D., Robertson, B., Tacchella, S., Alberts, S., Baker, W.M., Bhatawdekar, R., Boyett, K., Bunker, A.J., Cameron, A.J., Carniani, S., Charlot, S., Chen, Z., Chevallard, J., Curtis-Lake, E., Danhaive, A.L., Egami, E., Eisenstein, D.J., Hainline, K., Helton, J.M., Ji, Z., Looser, T.J., Maiolino, R., Nelson, E., Puskás, D., Rieke, G., Rieke, M., Rix, H.-W., Sandles, L., Saxena, A., Simmonds, C., Smit, R., Sun, F., Williams, C.C., Willmer, C.N.A., Willott, C., Witstok, J.: The Star-forming and Ionizing Properties of Dwarf $z \sim 6-9$ Galaxies in JADES: Insights on Bursty Star Formation and Ionized Bubble Growth. *arXiv e-prints*, 2306–05295 (2023) <https://doi.org/10.48550/arXiv.2306.05295> [arXiv:2306.05295](https://arxiv.org/abs/2306.05295) [astro-ph.GA]
- [9] Leitherer, C., Schaerer, D., Goldader, J.D., Delgado, R.M.G., Robert, C., Kune, D.F., de Mello, D.F., Devost, D., Heckman, T.M.: Starburst99: Synthesis Models for Galaxies with Active Star Formation. *ApJS* **123**(1), 3–40 (1999) <https://doi.org/10.1086/313233> [arXiv:astro-ph/9902334](https://arxiv.org/abs/astro-ph/9902334) [astro-ph]

- [10] Schaerer, D.: On the properties of massive Population III stars and metal-free stellar populations. *A&A* **382**, 28–42 (2002) <https://doi.org/10.1051/0004-6361:20011619> [arXiv:astro-ph/0110697](#) [astro-ph]
- [11] Raiter, A., Schaerer, D., Fosbury, R.A.E.: Predicted UV properties of very metal-poor starburst galaxies. *A&A* **523**, 64 (2010) <https://doi.org/10.1051/0004-6361/201015236> [arXiv:1008.2114](#) [astro-ph.CO]
- [12] Zackrisson, E., Rydberg, C.-E., Schaerer, D., Östlin, G., Tuli, M.: The Spectral Evolution of the First Galaxies. I. James Webb Space Telescope Detection Limits and Color Criteria for Population III Galaxies. *ApJ* **740**(1), 13 (2011) <https://doi.org/10.1088/0004-637X/740/1/13> [arXiv:1105.0921](#) [astro-ph.CO]
- [13] Miralda-Escudé, J.: Reionization of the Intergalactic Medium and the Damping Wing of the Gunn-Peterson Trough. *ApJ* **501**(1), 15–22 (1998) <https://doi.org/10.1086/305799> [arXiv:astro-ph/9708253](#) [astro-ph]
- [14] Heintz, K.E., Watson, D., Brammer, G., Vejlgaard, S., Hutter, A., Strait, V.B., Matthee, J., Oesch, P.A., Jakobsson, P., Tanvir, N.R., Laursen, P., Naidu, R.P., Mason, C.A., Killi, M., Jung, I., Hsiao, T.Y.-Y., Abdurro’uf, Coe, D., Arrabal Haro, P., Finkelstein, S.L., Toft, S.: Extreme damped Lyman- α absorption in young star-forming galaxies at $z = 9 - 11$. *arXiv e-prints*, 2306–00647 (2023) <https://doi.org/10.48550/arXiv.2306.00647> [arXiv:2306.00647](#) [astro-ph.GA]
- [15] Fosbury, R.A.E., Villar-Martín, M., Humphrey, A., Lombardi, M., Rosati, P., Stern, D., Hook, R.N., Holden, B.P., Stanford, S.A., Squires, G.K., Rauch, M., Sargent, W.L.W.: Massive Star Formation in a Gravitationally Lensed H II Galaxy at $z = 3.357$. *ApJ* **596**(2), 797–809 (2003) <https://doi.org/10.1086/378228> [arXiv:astro-ph/0307162](#) [astro-ph]
- [16] Bezanson, R., Labbe, I., Whitaker, K.E., Leja, J., Price, S.H., Franx, M., Brammer, G., Marchesini, D., Zitrin, A., Wang, B., Weaver, J.R., Furtak, L.J., Atek, H., Coe, D., Cutler, S.E., Dayal, P., van Dokkum, P., Feldmann, R., Forster Schreiber, N., Fujimoto, S., Geha, M., Glazebrook, K., de Graaff, A., Greene, J.E., Juneau, S., Kassin, S., Kriek, M., Khullar, G., Maseda, M., Mowla, L.A., Muzzin, A., Nanayakkara, T., Nelson, E.J., Oesch, P.A., Pacifici, C., Pan, R., Papovich, C., Setton, D., Shapley, A.E., Smit, R., Stefanon, M., Taylor, E.N., Williams, C.C.: The JWST UNCOVER Treasury survey: Ultradeep NIRSpect and NIRCams Observations before the Epoch of Reionization. *arXiv e-prints*, 2212–04026 (2022) <https://doi.org/10.48550/arXiv.2212.04026> [arXiv:2212.04026](#) [astro-ph.GA]
- [17] Bressan, A., Marigo, P., Girardi, L., Salasnich, B., Dal Cero, C., Rubele, S., Nanni, A.: PARSEC: stellar tracks and isochrones with the PAdova and TRieste Stellar Evolution Code. *MNRAS* **427**(1), 127–145 (2012) <https://doi.org/10.1111/j.1365-2966.2012.21948.x> [arXiv:1208.4498](#) [astro-ph.SR]
- [18] Maiolino, R., Scholtz, J., Witstok, J., Carniani, S., D’Eugenio, F., de Graaff,

- A., Uebler, H., Tacchella, S., Curtis-Lake, E., Arribas, S., Bunker, A., Charlot, S., Chevallard, J., Curti, M., Looser, T.J., Maseda, M.V., Rawle, T., Rodriguez Del Pino, B., Willott, C.J., Egami, E., Eisenstein, D., Hainline, K., Robertson, B., Williams, C.C., Willmer, C.N.A., Baker, W.M., Boyett, K., DeCoursey, C., Fabian, A.C., Helton, J.M., Ji, Z., Jones, G.C., Kumari, N., Laporte, N., Nelson, E., Perna, M., Sandles, L., Shivaiei, I., Sun, F.: A small and vigorous black hole in the early Universe. arXiv e-prints, 2305–12492 (2023) <https://doi.org/10.48550/arXiv.2305.12492> [astro-ph.GA]
- [19] Katz, H., Saxena, A., Cameron, A.J., Carniani, S., Bunker, A.J., Arribas, S., Bhatawdekar, R., Bowler, R.A.A., Boyett, K.N.K., Cresci, G., Curtis-Lake, E., D’Eugenio, F., Kumari, N., Looser, T.J., Maiolino, R., Uebler, H., Willott, C., Witstok, J.: First insights into the ISM at $z \lesssim 8$ with JWST: possible physical implications of a high [O III] $\lambda 4363$ /[O III] $\lambda 5007$. MNRAS **518**(1), 592–603 (2023) <https://doi.org/10.1093/mnras/stac2657> arXiv:2207.13693 [astro-ph.GA]
- [20] Binette, L., Groves, B., Villar-Martín, M., Fosbury, R.A.E., Axon, D.J.: High- z nebulae: Ionization by stars or by an obscured QSO? A&A **405**, 975–980 (2003) <https://doi.org/10.1051/0004-6361:20030718>
- [21] Klessen, R.S., Glover, S.C.O.: The First Stars: Formation, Properties, and Impact. ARA&A **61**, 65–130 (2023) <https://doi.org/10.1146/annurev-astro-071221-053453> arXiv:2303.12500 [astro-ph.CO]
- [22] Larkin, M.M., Gerasimov, R., Burgasser, A.J.: Characterization of Population III Stars with Stellar Atmosphere and Evolutionary Modeling and Predictions of their Observability with the JWST. AJ **165**(1), 2 (2023) <https://doi.org/10.3847/1538-3881/ac9b43> arXiv:2210.09185 [astro-ph.SR]
- [23] Götzberg, Y., de Mink, S.E., Groh, J.H., Kupfer, T., Crowther, P.A., Zapartas, E., Renzo, M.: Spectral models for binary products: Unifying subdwarfs and Wolf-Rayet stars as a sequence of stripped-envelope stars. A&A **615**, 78 (2018) <https://doi.org/10.1051/0004-6361/201732274> arXiv:1802.03018 [astro-ph.SR]
- [24] Todt, H., Sander, A., Hainich, R., Hamann, W.-R., Quade, M., Shenar, T.: Potsdam Wolf-Rayet model atmosphere grids for WN stars. A&A **579**, 75 (2015) <https://doi.org/10.1051/0004-6361/201526253>
- [25] Olivier, G.M., Berg, D.A., Chisholm, J., Erb, D.K., Pogge, R.W., Skillman, E.D.: Characterizing Extreme Emission Line Galaxies. II. A Self-consistent Model of Their Ionizing Spectrum. ApJ **938**(1), 16 (2022) <https://doi.org/10.3847/1538-4357/ac8f2c> arXiv:2109.06725 [astro-ph.GA]
- [26] Massey, P., DeGioia-Eastwood, K., Waterhouse, E.: The Progenitor Masses of Wolf-Rayet Stars and Luminous Blue Variables Determined from Cluster Turnoffs. II. Results from 12 Galactic Clusters and OB Associations. AJ **121**(2),

- 1050–1070 (2001) <https://doi.org/10.1086/318769> arXiv:astro-ph/0010654 [astro-ph]
- [27] Hainich, R., Pasemann, D., Todt, H., Shenar, T., Sander, A., Hamann, W.-R.: Wolf-Rayet stars in the Small Magellanic Cloud. I. Analysis of the single WN stars. *A&A* **581**, 21 (2015) <https://doi.org/10.1051/0004-6361/201526241> arXiv:1507.04000 [astro-ph.SR]
- [28] Katz, H., Rosdahl, J., Kimm, T., Garel, T., Blaizot, J., Haehnelt, M.G., Michel-Dansac, L., Martin-Alvarez, S., Devriendt, J., Slyz, A., Teyssier, R., Ocvirk, P., Laporte, N., Ellis, R.: The nature of high $[\text{O III}]_{88\mu\text{m}}/[\text{C II}]_{158\mu\text{m}}$ galaxies in the epoch of reionization: Low carbon abundance and a top-heavy IMF? *MNRAS* **510**(4), 5603–5622 (2022) <https://doi.org/10.1093/mnras/stac028> arXiv:2108.01074 [astro-ph.GA]
- [29] Finkelstein, S.L., Bagley, M.B., Ferguson, H.C., Wilkins, S.M., Kartaltepe, J.S., Papovich, C., Yung, L.Y.A., Arrabal Haro, P., Behroozi, P., Dickinson, M., Kocevski, D.D., Koekemoer, A.M., Larson, R.L., Le Bail, A., Morales, A.M., Pérez-González, P.G., Burgarella, D., Davé, R., Hirschmann, M., Somerville, R.S., Wuyts, S., Bromm, V., Casey, C.M., Fontana, A., Fujimoto, S., Gardner, J.P., Giavalisco, M., Grazian, A., Grogin, N.A., Hathi, N.P., Hutchison, T.A., Jha, S.W., Jogee, S., Kewley, L.J., Kirkpatrick, A., Long, A.S., Lotz, J.M., Pentericci, L., Pierel, J.D.R., Pirzkal, N., Ravindranath, S., Ryan, R.E., Trump, J.R., Yang, G., Bhatawdekar, R., Bisigello, L., Buat, V., Calabrò, A., Castellano, M., Cleri, N.J., Cooper, M.C., Croton, D., Daddi, E., Dekel, A., Elbaz, D., Franco, M., Gawiser, E., Holwerda, B.W., Huertas-Company, M., Jaskot, A.E., Leung, G.C.K., Lucas, R.A., Mobasher, B., Pandya, V., Tacchella, S., Weiner, B.J., Zavala, J.A.: CEERS Key Paper. I. An Early Look into the First 500 Myr of Galaxy Formation with JWST. *ApJ* **946**(1), 13 (2023) <https://doi.org/10.3847/2041-8213/acade4> arXiv:2211.05792 [astro-ph.GA]
- [30] Robertson, B.E., Furlanetto, S.R., Schneider, E., Charlot, S., Ellis, R.S., Stark, D.P., McLure, R.J., Dunlop, J.S., Koekemoer, A., Schenker, M.A., Ouchi, M., Ono, Y., Curtis-Lake, E., Rogers, A.B., Bowler, R.A.A., Cirasuolo, M.: New Constraints on Cosmic Reionization from the 2012 Hubble Ultra Deep Field Campaign. *ApJ* **768**(1), 71 (2013) <https://doi.org/10.1088/0004-637X/768/1/71> arXiv:1301.1228 [astro-ph.CO]
- [31] Eisenstein, D.J., Willott, C., Albers, S., Arribas, S., Bonaventura, N., Bunker, A.J., Cameron, A.J., Carniani, S., Charlot, S., Curtis-Lake, E., D’Eugenio, F., Endsley, R., Ferruit, P., Giardino, G., Hainline, K., Hausen, R., Jakobsen, P., Johnson, B.D., Maiolino, R., Rieke, M., Rieke, G., Rix, H.-W., Robertson, B., Stark, D.P., Tacchella, S., Williams, C.C., Willmer, C.N.A., Baker, W.M., Baum, S., Bhatawdekar, R., Boyett, K., Chen, Z., Chevallard, J., Circosta, C., Curti, M., Danhaive, A.L., DeCoursey, C., de Graaff, A., Dressler, A., Egami, E., Helton, J.M., Hviding, R.E., Ji, Z., Jones, G.C., Kumari, N., Lützgendorf, N., Laseter,

- I., Looser, T.J., Lyu, J., Maseda, M.V., Nelson, E., Parlanti, E., Perna, M., Puskás, D., Rawle, T., Rodríguez Del Pino, B., Sandles, L., Saxena, A., Scholtz, J., Sharpe, K., Shivaiei, I., Silcock, M.S., Simmonds, C., Skarbinski, M., Smit, R., Stone, M., Suess, K.A., Sun, F., Tang, M., Topping, M.W., Übler, H., Villanueva, N.C., Wallace, I.E.B., Whitler, L., Witstok, J., Woodrum, C.: Overview of the JWST Advanced Deep Extragalactic Survey (JADES). arXiv e-prints, 2306–02465 (2023) <https://doi.org/10.48550/arXiv.2306.02465> arXiv:2306.02465 [astro-ph.GA]
- [32] Bunker, A.J., Cameron, A.J., Curtis-Lake, E., Jakobsen, P., Carniani, S., Curti, M., Witstok, J., Maiolino, R., D’Eugenio, F., Looser, T.J., Willott, C., Bonaventura, N., Hainline, K., Uebler, H., Willmer, C.N.A., Saxena, A., Smit, R., Alberts, S., Arribas, S., Baker, W.M., Baum, S., Bhatawdekar, R., Bowler, R.A.A., Boyett, K., Charlot, S., Chen, Z., Chevallard, J., Circosta, C., DeCoursey, C., de Graaff, A., Egami, E., Eisenstein, D.J., Endsley, R., Ferruit, P., Giardino, G., Hausen, R., Helton, J.M., Hviding, R.E., Ji, Z., Johnson, B.D., Jones, G.C., Kumari, N., Laseter, I., Luetzgendorf, N., Maseda, M.V., Nelson, E., Parlanti, E., Perna, M., Rawle, T., Rix, H.-W., Rieke, M., Robertson, B., Rodríguez Del Pino, B., Sandles, L., Scholtz, J., Sharpe, K., Skarbinski, M., Stark, D.P., Sun, F., Tacchella, S., Topping, M.W., Villanueva, N.C., Wallace, I.E.B., Williams, C.C., Woodrum, C.: JADES NIRSpec Initial Data Release for the Hubble Ultra Deep Field: Redshifts and Line Fluxes of Distant Galaxies from the Deepest JWST Cycle 1 NIRSpec Multi-Object Spectroscopy. arXiv e-prints, 2306–02467 (2023) <https://doi.org/10.48550/arXiv.2306.02467> arXiv:2306.02467 [astro-ph.GA]
- [33] Bezanson, R., Labbe, I., Whitaker, K.E., Leja, J., Price, S.H., Franx, M., Brammer, G., Marchesini, D., Zitrin, A., Wang, B., Weaver, J.R., Furtak, L.J., Atek, H., Coe, D., Cutler, S.E., Dayal, P., van Dokkum, P., Feldmann, R., Forster Schreiber, N., Fujimoto, S., Geha, M., Glazebrook, K., de Graaff, A., Greene, J.E., Juneau, S., Kassin, S., Kriek, M., Khullar, G., Maseda, M., Mowla, L.A., Muzzin, A., Nanayakkara, T., Nelson, E.J., Oesch, P.A., Pacifici, C., Pan, R., Papovich, C., Setton, D., Shapley, A.E., Smit, R., Stefanon, M., Taylor, E.N., Williams, C.C.: The JWST UNCOVER Treasury survey: Ultradeep NIRSpec and NIRCам Observations before the Epoch of Reionization. arXiv e-prints, 2212–04026 (2022) <https://doi.org/10.48550/arXiv.2212.04026> arXiv:2212.04026 [astro-ph.GA]
- [34] Bergamini, P., Acebron, A., Grillo, C., Rosati, P., Caminha, G.B., Mercurio, A., Vanzella, E., Mason, C., Treu, T., Angora, G., Brammer, G.B., Meneghetti, M., Nonino, M., Boyett, K., Bradač, M., Castellano, M., Fontana, A., Morishita, T., Paris, D., Prieto-Lyon, G., Roberts-Borsani, G., Roy, N., Santini, P., Vulcani, B., Wang, X., Yang, L.: The GLASS-JWST Early Release Science Program. III. Strong-lensing Model of Abell 2744 and Its Infalling Regions. *ApJ* **952**(1), 84 (2023) <https://doi.org/10.3847/1538-4357/acd643> arXiv:2303.10210 [astro-ph.GA]
- [35] Heintz, K.E., Watson, D., Brammer, G., Vejlgaard, S., Hutter, A., Strait, V.B.,

- Matthee, J., Oesch, P.A., Jakobsson, P., Tanvir, N.R., Laursen, P., Naidu, R.P., Mason, C.A., Killi, M., Jung, I., Hsiao, T.Y.-Y., Abdurro'uf, Coe, D., Arrabal Haro, P., Finkelstein, S.L., Toft, S.: Extreme damped Lyman- α absorption in young star-forming galaxies at $z = 9 - 11$. arXiv e-prints, 2306–00647 (2023) <https://doi.org/10.48550/arXiv.2306.00647> arXiv:2306.00647 [astro-ph.GA]
- [36] Luridiana, V., Morisset, C., Shaw, R.A.: PyNeb: a new tool for analyzing emission lines. I. Code description and validation of results. *A&A* **573**, 42 (2015) <https://doi.org/10.1051/0004-6361/201323152> arXiv:1410.6662 [astro-ph.IM]
- [37] Dere, K.P., Landi, E., Mason, H.E., Monsignori Fossi, B.C., Young, P.R.: CHIANTI - an atomic database for emission lines. *A&AS* **125**, 149–173 (1997) <https://doi.org/10.1051/aas:1997368>
- [38] Del Zanna, G., Dere, K.P., Young, P.R., Landi, E.: CHIANTI—An Atomic Database for Emission Lines. XVI. Version 10, Further Extensions. *ApJ* **909**(1), 38 (2021) <https://doi.org/10.3847/1538-4357/abd8ce> arXiv:2011.05211 [physics.atom-ph]
- [39] Pérez-Montero, E.: Ionized Gaseous Nebulae Abundance Determination from the Direct Method. *PASP* **129**(974), 043001 (2017) <https://doi.org/10.1088/1538-3873/aa5abb> arXiv:1702.04255 [astro-ph.GA]
- [40] Cameron, A.J., Katz, H., Rey, M.P., Saxena, A.: Nitrogen enhancements 440 Myr after the big bang: supersolar N/O, a tidal disruption event, or a dense stellar cluster in GN-z11? *MNRAS* **523**(3), 3516–3525 (2023) <https://doi.org/10.1093/mnras/stad1579> arXiv:2302.10142 [astro-ph.GA]
- [41] Amayo, A., Delgado-Inglada, G., Stasińska, G.: Ionization correction factors and dust depletion patterns in giant H II regions. *MNRAS* **505**(2), 2361–2376 (2021) <https://doi.org/10.1093/mnras/stab1467> arXiv:2105.08891 [astro-ph.GA]
- [42] Berg, D.A., Erb, D.K., Henry, R.B.C., Skillman, E.D., McQuinn, K.B.W.: The Chemical Evolution of Carbon, Nitrogen, and Oxygen in Metal-poor Dwarf Galaxies. *ApJ* **874**(1), 93 (2019) <https://doi.org/10.3847/1538-4357/ab020a> arXiv:1901.08160 [astro-ph.GA]
- [43] Matsumoto, A., Ouchi, M., Nakajima, K., Kawasaki, M., Murai, K., Motohara, K., Harikane, Y., Ono, Y., Kushibiki, K., Koyama, S., Aoyama, S., Konishi, M., Takahashi, H., Isobe, Y., Umeda, H., Sugahara, Y., Onodera, M., Nagamine, K., Kusakabe, H., Hirai, Y., Moriya, T.J., Shibuya, T., Komiyama, Y., Fukushima, K., Fujimoto, S., Hattori, T., Hayashi, K., Inoue, A.K., Kikuchihara, S., Kojima, T., Koyama, Y., Lee, C.-H., Mawatari, K., Miyata, T., Nagao, T., Ozaki, S., Rauch, M., Saito, T., Suzuki, A., Takeuchi, T.T., Umemura, M., Xu, Y., Yabe, K., Zhang, Y., Yoshii, Y.: EMPRESS. VIII. A New Determination of Primordial He Abundance with Extremely Metal-poor Galaxies: A Suggestion of the Lepton Asymmetry and Implications for the Hubble Tension. *ApJ* **941**(2), 167 (2022)

<https://doi.org/10.3847/1538-4357/ac9ea1> arXiv:2203.09617 [astro-ph.CO]

- [44] Piotto, G., Bedin, L.R., Anderson, J., King, I.R., Cassisi, S., Milone, A.P., Villanova, S., Pietrinferni, A., Renzini, A.: A Triple Main Sequence in the Globular Cluster NGC 2808. *ApJ* **661**(1), 53–56 (2007) <https://doi.org/10.1086/518503> arXiv:astro-ph/0703767 [astro-ph]
- [45] Peimbert, M., Torres-Peimbert, S., Ruiz, M.T.: The chemical composition of the galactic H II region M17. *Rev. Mexicana Astron. Astrofis.* **24**, 155–177 (1992)
- [46] Hu, W., Martin, C.L., Gronke, M., Gazagnes, S., Hayes, M., Chisholm, J., Heckman, T., Mingozi, M., Roy, N., Senchyna, P., Xu, X., Berg, D.A., James, B.L., Stark, D.P., Arellano-Córdova, K.Z., Henry, A., Jaskot, A.E., Kumari, N., Parker, K.S., Scarlata, C., Wofford, A., Amorín, R.O., Leonhardes-Barboza, N., Brinchmann, J., Carr, C., Aloisi, A.: CLASSY VII Ly α Profiles: The Structure and Kinematics of Neutral Gas and Implications for LyC Escape in Reionization-era Analogs. *ApJ* **956**(1), 39 (2023) <https://doi.org/10.3847/1538-4357/aceefd> arXiv:2307.04911 [astro-ph.GA]
- [47] Tanvir, N.R., Fynbo, J.P.U., de Ugarte Postigo, A., Japelj, J., Wiersema, K., Malesani, D., Perley, D.A., Levan, A.J., Selsing, J., Cenko, S.B., Kann, D.A., Milvang-Jensen, B., Berger, E., Cano, Z., Chornock, R., Covino, S., Cucchiara, A., D’Elia, V., Gargiulo, A., Goldoni, P., Gomboc, A., Heintz, K.E., Hjorth, J., Izzo, L., Jakobsson, P., Kaper, L., Krühler, T., Laskar, T., Myers, M., Piranomonte, S., Pugliese, G., Rossi, A., Sánchez-Ramírez, R., Schulze, S., Sparre, M., Stanway, E.R., Tagliaferri, G., Thöne, C.C., Vergani, S., Vreeswijk, P.M., Wijers, R.A.M.J., Watson, D., Xu, D.: The fraction of ionizing radiation from massive stars that escapes to the intergalactic medium. *MNRAS* **483**(4), 5380–5408 (2019) <https://doi.org/10.1093/mnras/sty3460> arXiv:1805.07318 [astro-ph.GA]
- [48] Umeda, H., Ouchi, M., Nakajima, K., Harikane, Y., Ono, Y., Xu, Y., Isobe, Y., Zhang, Y.: JWST Measurements of Neutral Hydrogen Fractions and Ionized Bubble Sizes at $z = 7 - 12$ Obtained with Ly α Damping Wing Absorptions in 26 Bright Continuum Galaxies. arXiv e-prints, 2306–00487 (2023) <https://doi.org/10.48550/arXiv.2306.00487> arXiv:2306.00487 [astro-ph.GA]
- [49] Ferland, G.J., Chatzikos, M., Guzmán, F., Lykins, M.L., van Hoof, P.A.M., Williams, R.J.R., Abel, N.P., Badnell, N.R., Keenan, F.P., Porter, R.L., Stancil, P.C.: The 2017 Release Cloudy. *Rev. Mexicana Astron. Astrofis.* **53**, 385–438 (2017) <https://doi.org/10.48550/arXiv.1705.10877> arXiv:1705.10877 [astro-ph.GA]
- [50] Eldridge, J.J., Stanway, E.R., Xiao, L., McClelland, L.A.S., Taylor, G., Ng, M., Greis, S.M.L., Bray, J.C.: Binary Population and Spectral Synthesis Version 2.1: Construction, Observational Verification, and New Results. *PASA* **34**, 058 (2017) <https://doi.org/10.1017/pasa.2017.51> arXiv:1710.02154 [astro-ph.SR]

- [51] Verhamme, A., Orlitová, I., Schaerer, D., Hayes, M.: Using Lyman- α to detect galaxies that leak Lyman continuum. *A&A* **578**, 7 (2015) <https://doi.org/10.1051/0004-6361/201423978> [arXiv:1404.2958](https://arxiv.org/abs/1404.2958) [astro-ph.GA]
- [52] Grevesse, N., Asplund, M., Sauval, A.J., Scott, P.: The chemical composition of the Sun. *Ap&SS* **328**(1-2), 179–183 (2010) <https://doi.org/10.1007/s10509-010-0288-z>
- [53] Garel, T., Blaizot, J., Rosdahl, J., Michel-Dansac, L., Haehnelt, M.G., Katz, H., Kimm, T., Verhamme, A.: Ly α as a tracer of cosmic reionization in the SPHINX radiation-hydrodynamics cosmological simulation. *MNRAS* **504**(2), 1902–1926 (2021) <https://doi.org/10.1093/mnras/stab990> [arXiv:2104.03339](https://arxiv.org/abs/2104.03339) [astro-ph.GA]
- [54] Barkana, R., Loeb, A.: In the beginning: the first sources of light and the reionization of the universe. *Phys. Rep.* **349**(2), 125–238 (2001) [https://doi.org/10.1016/S0370-1573\(01\)00019-9](https://doi.org/10.1016/S0370-1573(01)00019-9) [arXiv:astro-ph/0010468](https://arxiv.org/abs/astro-ph/0010468) [astro-ph]
- [55] Guzmán, F., Badnell, N.R., Chatzikos, M., van Hoof, P.A.M., Williams, R.J.R., Ferland, G.J.: Testing atomic collision theory with the two-photon continuum of astrophysical nebulae. *MNRAS* **467**(4), 3944–3950 (2017) <https://doi.org/10.1093/mnras/stx269> [arXiv:1701.07913](https://arxiv.org/abs/1701.07913) [astro-ph.CO]
- [56] Kobayashi, C., Karakas, A.I., Lugaro, M.: The Origin of Elements from Carbon to Uranium. *ApJ* **900**(2), 179 (2020) <https://doi.org/10.3847/1538-4357/abae65> [arXiv:2008.04660](https://arxiv.org/abs/2008.04660) [astro-ph.GA]
- [57] Senchyna, P., Stark, D.P., Mirocha, J., Reines, A.E., Charlot, S., Jones, T., Mulchaey, J.S.: High-mass X-ray binaries in nearby metal-poor galaxies: on the contribution to nebular He II emission. *MNRAS* **494**(1), 941–957 (2020) <https://doi.org/10.1093/mnras/staa586> [arXiv:1909.10574](https://arxiv.org/abs/1909.10574) [astro-ph.GA]
- [58] Mitsuda, K., Inoue, H., Koyama, K., Makishima, K., Matsuoka, M., Ogawara, Y., Shibazaki, N., Suzuki, K., Tanaka, Y., Hirano, T.: Energy spectra of low-mass binary X-ray sources observed from Tenma. *PASJ* **36**, 741–759 (1984)
- [59] Gräfener, G., Hamann, W.-R.: Mass loss from late-type WN stars and its Z-dependence. Very massive stars approaching the Eddington limit. *A&A* **482**(3), 945–960 (2008) <https://doi.org/10.1051/0004-6361/20066176> [arXiv:0803.0866](https://arxiv.org/abs/0803.0866) [astro-ph]
- [60] Gräfener, G., Vink, J.S.: Narrow He II emission in star-forming galaxies at low metallicity. Stellar wind emission from a population of very massive stars. *A&A* **578**, 2 (2015) <https://doi.org/10.1051/0004-6361/201425287> [arXiv:1505.02994](https://arxiv.org/abs/1505.02994) [astro-ph.GA]
- [61] Planck Collaboration, Ade, P.A.R., Aghanim, N., Arnaud, M., Ashdown, M.,

Aumont, J., Baccigalupi, C., Banday, A.J., Barreiro, R.B., Bartlett, J.G., Bartolo, N., Battaner, E., Battye, R., Benabed, K., Benoît, A., Benoît-Lévy, A., Bernard, J.-P., Bersanelli, M., Bielewicz, P., Bock, J.J., Bonaldi, A., Bonavera, L., Bond, J.R., Borrill, J., Bouchet, F.R., Boulanger, F., Bucher, M., Burigana, C., Butler, R.C., Calabrese, E., Cardoso, J.-F., Catalano, A., Challinor, A., Chamba-llu, A., Chary, R.-R., Chiang, H.C., Chluba, J., Christensen, P.R., Church, S., Clements, D.L., Colombi, S., Colombo, L.P.L., Combet, C., Coulais, A., Crill, B.P., Curto, A., Cuttaia, F., Danese, L., Davies, R.D., Davis, R.J., de Bernardis, P., de Rosa, A., de Zotti, G., Delabrouille, J., Désert, F.-X., Di Valentino, E., Dickinson, C., Diego, J.M., Dolag, K., Dole, H., Donzelli, S., Doré, O., Douspis, M., Ducout, A., Dunkley, J., Dupac, X., Efstathiou, G., Elsner, F., Enßlin, T.A., Eriksen, H.K., Farhang, M., Fergusson, J., Finelli, F., Forni, O., Frailis, M., Fraisse, A.A., Franceschi, E., Frejsel, A., Galeotta, S., Galli, S., Ganga, K., Gauthier, C., Gerbino, M., Ghosh, T., Giard, M., Giraud-Héraud, Y., Giusarma, E., Gjerløw, E., González-Nuevo, J., Górski, K.M., Gratton, S., Gregorio, A., Gruppuso, A., Gudmundsson, J.E., Hamann, J., Hansen, F.K., Hanson, D., Harrison, D.L., Helou, G., Henrot-Versillé, S., Hernández-Monteagudo, C., Herranz, D., Hildebrandt, S.R., Hivon, E., Hobson, M., Holmes, W.A., Hornstrup, A., Hovest, W., Huang, Z., Huppenberger, K.M., Hurier, G., Jaffe, A.H., Jaffe, T.R., Jones, W.C., Juvela, M., Keihänen, E., Keskitalo, R., Kisner, T.S., Kneissl, R., Knoche, J., Knox, L., Kunz, M., Kurki-Suonio, H., Lagache, G., Lähteenmäki, A., Lamarre, J.-M., Lasenby, A., Lattanzi, M., Lawrence, C.R., Leahy, J.P., Leonardi, R., Lesgourgues, J., Levrier, F., Lewis, A., Liguori, M., Lilje, P.B., Linden-Vørnle, M., López-Caniego, M., Lubin, P.M., Macías-Pérez, J.F., Maggio, G., Maino, D., Mandolesi, N., Mangilli, A., Marchini, A., Maris, M., Martin, P.G., Martinelli, M., Martínez-González, E., Masi, S., Matarrese, S., McGehee, P., Meinhold, P.R., Melchiorri, A., Melin, J.-B., Mendes, L., Mennella, A., Migliaccio, M., Millea, M., Mitra, S., Miville-Deschênes, M.-A., Moneti, A., Montier, L., Morgante, G., Mortlock, D., Moss, A., Munshi, D., Murphy, J.A., Naselsky, P., Nati, F., Natoli, P., Netterfield, C.B., Nørgaard-Nielsen, H.U., Noviello, F., Novikov, D., Novikov, I., Oxborrow, C.A., Paci, F., Pagano, L., Pajot, F., Paladini, R., Paoletti, D., Partridge, B., Pasian, F., Patanchon, G., Pearson, T.J., Perdureau, O., Perotto, L., Perrotta, F., Pettorino, V., Piacentini, F., Piat, M., Pierpaoli, E., Pietrobon, D., Plaszczynski, S., Pointecouteau, E., Polenta, G., Popa, L., Pratt, G.W., Prézeau, G., Prunet, S., Puget, J.-L., Rachen, J.P., Reach, W.T., Rebolo, R., Reinecke, M., Remazeilles, M., Renault, C., Renzi, A., Ristorcelli, I., Rocha, G., Rosset, C., Rossetti, M., Roudier, G., Rouillé d'Orfeuil, B., Rowan-Robinson, M., Rubiño-Martín, J.A., Rusholme, B., Said, N., Salvatelli, V., Salvati, L., Sandri, M., Santos, D., Savelainen, M., Savini, G., Scott, D., Seiffert, M.D., Serra, P., Shellard, E.P.S., Spencer, L.D., Spinelli, M., Stolyarov, V., Stompor, R., Sudiwala, R., Sunyaev, R., Sutton, D., Suur-Uski, A.-S., Sygnet, J.-F., Tauber, J.A., Terenzi, L., Toffolatti, L., Tomasi, M., Tristram, M., Trombetti, T., Tucci, M., Tuovinen, J., Türler, M., Umana, G., Valenziano, L., Valiviita, J., Van Tent, F., Vielva, P., Villa, F., Wade, L.A., Wandelt, B.D., Wehus, I.K., White, M., White, S.D.M., Wilkinson, A., Yvon, D., Zacchei, A., Zonca, A.: Planck 2015 results. XIII. Cosmological

parameters. A&A **594**, 13 (2016) <https://doi.org/10.1051/0004-6361/201525830>
[arXiv:1502.01589](https://arxiv.org/abs/1502.01589) [astro-ph.CO]

- [62] Osterbrock, D.E., Ferland, G.J.: Astrophysics of Gaseous Nebulae and Active Galactic Nuclei, (2006)

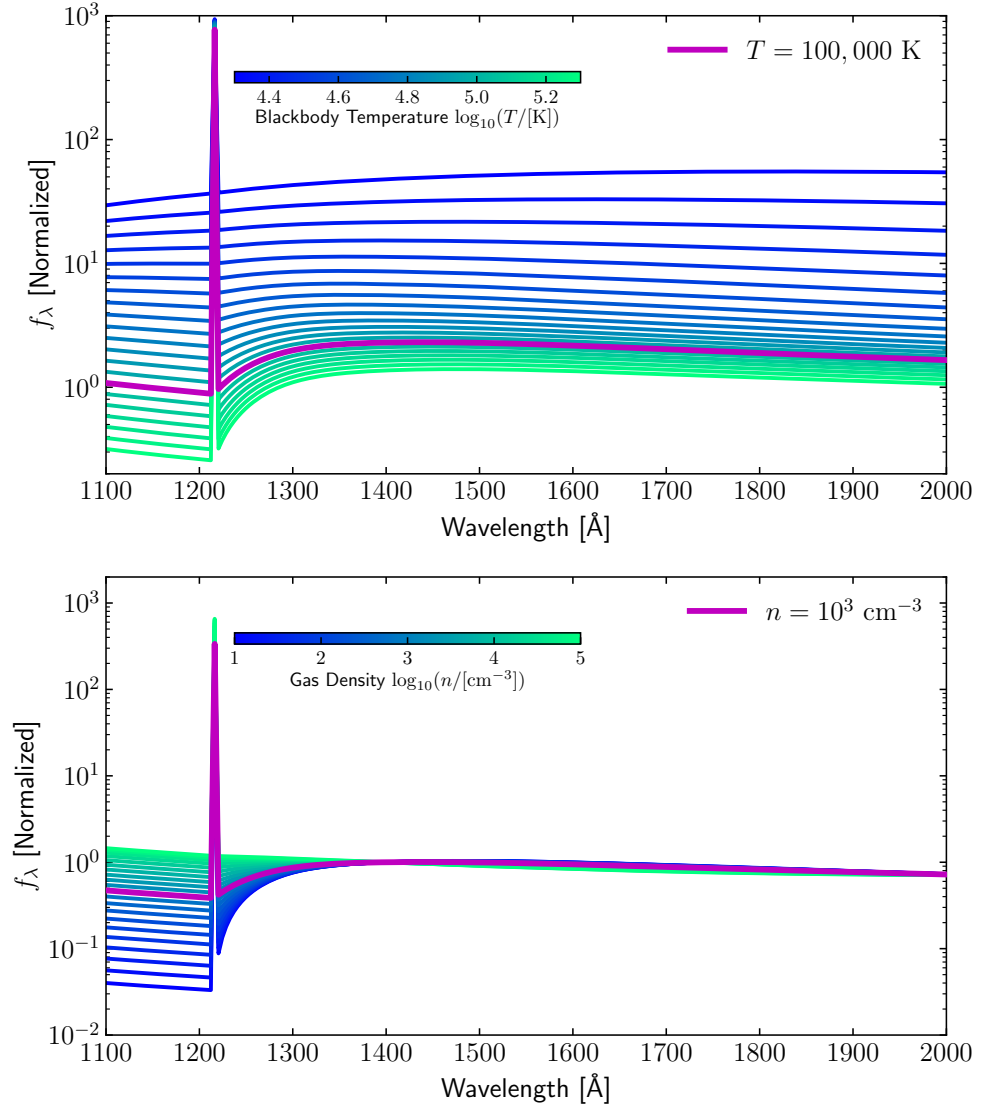


Fig. 8 (Top) Normalized spectrum of hydrogen-only gas with $n = 10^3$ cm $^{-3}$ irradiated by blackbodies of different temperatures (as given in the colour bar). The magenta line represents a blackbody temperature of 100,000 K. (Bottom) Normalized spectrum of hydrogen-only gas irradiated by a blackbody with $T = 10^5$ K at different gas densities (as given in the colour bar). The magenta line represents a density of 10^3 cm $^{-3}$.

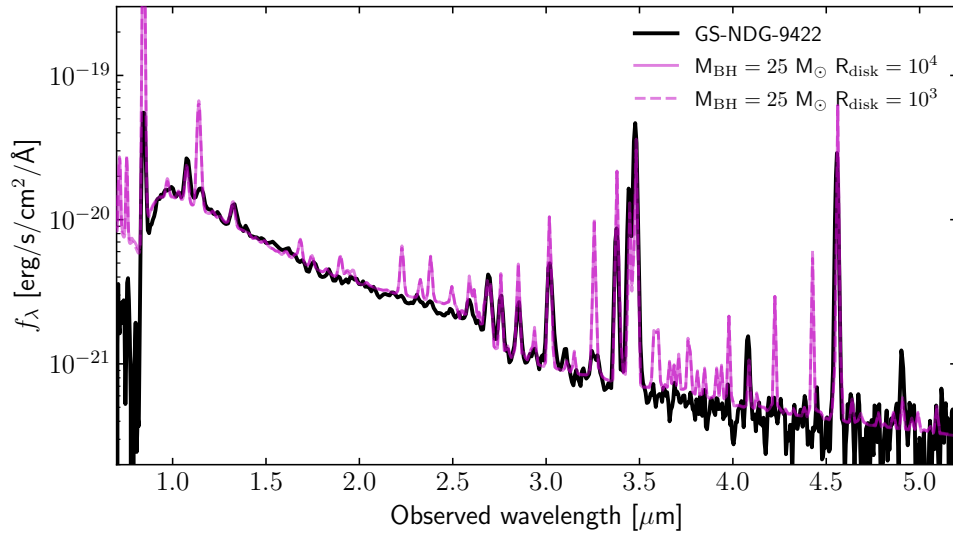


Fig. 9 JWST NIRSpec PRISM spectrum of GS-NDG-9422 (black) compared with photoionization models that include high-mass X-ray binaries with a black hole mass of $25 M_{\odot}$ (magenta). The solid and dashed magenta lines indicate models with different accretion disk radii.